


## Enhanced Cooper-Pair Injection into a Semiconductor Structure by Resonant Tunneling

Shlomi Bouscher<sup>✉</sup>, Dmitry Panna, Krishna Balasubramanian, Shimon Cohen, Dan Ritter, and Alex Hayat  
*Department of Electrical Engineering, Technion, Haifa 32000, Israel*

 (Received 3 June 2021; revised 2 January 2022; accepted 9 February 2022; published 24 March 2022)

We demonstrate enhanced Andreev reflection in a Nb/InGaAs/InP-based superconductor-semiconductor hybrid device resulting in increased Cooper-pair injection efficiency, achieved by Cooper-pair tunneling into a semiconductor quantum well resonant state. We show this enhancement by investigating the differential conductance spectra of two kinds of samples: one exhibiting resonant states and one which does not. We observe resonant features alongside strong enhancement of Cooper pair injection in the resonant sample, and lack of Cooper pair injection in the nonresonant sample. The theoretical modeling for measured spectra by a numerical approach agrees well with the experimental data. Our findings open a wide range of directions in condensed matter physics and in quantum technologies such as superconducting light-emitting diodes and structures supporting exotic excitations.

DOI: [10.1103/PhysRevLett.128.127701](https://doi.org/10.1103/PhysRevLett.128.127701)

Hybrid superconductor-semiconductor-based devices combine the technologically established field of semiconductors with the basic-science field of superconductors. Superconductors hold a plethora of unique properties such as zero electrical resistance and the Meissner effect [1]. Hybrid superconductor-semiconductor devices enable a variety of applications in rapidly developing fields such as quantum information processing and quantum communications. These applications include entangled photon pair generation via superconductor-coupled quantum dots [2,3], Bell-state analyzers [4], and two-photon amplification in waveguide amplifiers [5]. Furthermore, superconductor-semiconductor devices involving coupling of a superconductor with 2D electron gas has been well sought after, as they are predicted to have unique topological properties [6–11]. Another notable application is the superconducting light-emitting diode (SLED) [12–14], which radiatively recombines Cooper pairs with holes, emitting polarization-entangled photon pairs [15]. While Cooper pair injection from a superconductor into an *n*-type semiconducting layer [16–19] and into a light-emitting diode [20] has been previously demonstrated, the injection efficiency evident by the weak signature of Andreev reflection was low due to the potential barrier (Schottky barrier) and Fermi velocity mismatch [21], both of which inhibit Andreev reflection in favor of quasiparticle tunneling. Enhancing Cooper-pair injection into semiconducting materials allows for better coupling of the superconducting condensate with the multitude of options, which are present in the field of semiconductors such as SLEDs [12–15,17,20] for quantum light sources and exploring the physics of high- $T_c$  superconductors, by quantum optically probing the nature of Cooper pairs. Moreover, superconductor-semiconductor interfaces are crucial in the search for exotic excitations in semiconductors in proximity to superconductors [6,22,23].

Here, we demonstrate enhanced Andreev reflection by means of resonant tunneling enabling efficient Cooper pair injection. To corroborate this result, we use our previously developed numerical model [21], extending the BTK model to include arbitrary spatial potential barriers. Resonant tunneling, a phenomenon in which charge carriers are tunneling across a resonant energy state, resulting in an increase of the tunneling probability, has been utilized in resonant tunneling diodes [24,25] and quantum cascade lasers [26]. However, previously, this effect was shown only in one-electron transport, whereas here we use resonant tunneling of quasiparticle pairs in Andreev reflection, corresponding to enhanced Cooper-pair injection.

In order to demonstrate the effect of Andreev reflection enhancement by resonant tunneling, two suitable superconductor-semiconductor devices were grown using metal-organic molecular beam epitaxy for the semiconductor structure and sputtering for the superconductor layer (Table I). One device (resonant sample) was designed to have resonant quantum well (QW) energy levels, with the Fermi energy aligned with one of the levels [Fig. 3(a)], while the other sample (nonresonant sample) was designed to have a monotonic density of states without resonant QW energy levels. For both devices (Table I), the structure consists of an InP *N*-type side has an approximate thickness of  $\sim 90$  nm, with the Schottky barrier forming one side of the quantum well. On top of the *N*-type InP layer is an  $\text{In}_{0.53}\text{Ga}_{0.47}\text{As}$  layer, upon which the superconducting contact was deposited. For the resonant sample, the thickness of the  $\text{In}_{0.53}\text{Ga}_{0.47}\text{As}$  layer is  $\sim 10$  nm, which combined with the *N*-type InP layer, results in a  $\sim 100$  nm thick QW. For the nonresonant sample, the thickness of the  $\text{In}_{0.53}\text{Ga}_{0.47}\text{As}$  layer is  $\sim 300$  nm, resulting in a  $\sim 400$  nm thick well layer. For efficient Cooper-pair injection, good contact quality is required. In metal-semiconductor junctions, the presence

TABLE I. Device layout for resonant and nonresonant samples.

Layer	Material	Thickness (Å)	Doping (cm <sup>-3</sup> )
1. Superconductor	Nb	2000	NA <sup>a</sup>
2. Contact layer	In <sub>0.53</sub> Ga <sub>0.47</sub> As	100(resonant)/3000(nonresonant)	N-type 5 × 10 <sup>19</sup>
3. N-type layer/QW	InP	1000	N-type 5 × 10 <sup>19</sup>
4. Intrinsic layer	InP	500	NA
5. P-type substrate	InP	≫1000	P-type 1 × 10 <sup>18</sup>

<sup>a</sup>NA represents “not applicable”.

of a Schottky barrier, even for a resonant structure, can inhibit Cooper pair injection. Therefore, in both kinds of samples, a heavily doped In<sub>0.53</sub>Ga<sub>0.47</sub>As top layer reduces the width of the Schottky barrier [27]. Contacts were then fabricated and both devices were bonded and inserted into a suitable cryogenic environment. The lateral dimensions of the devices fabricated are 100 × 50 (μm<sup>2</sup>). Below  $T_c$ , the resistance of the superconductor vanishes. Therefore, the potential is expected to be equal along the lateral dimension of the pad, resulting in a uniform current density throughout the device, with negligible edge effects. The current distribution is close to uniform for temperatures above  $T_c$  as well, since the resistance of the superconducting pad in its metallic state is still very small (order of ~1 Ω).

Both devices were cooled to 3.2 K, with an obtained  $T_c$  of 7.8 K. Electrical four-probe transport measurements using a lock-in amplifier were then performed in order to obtain the differential conductance ( $dI/dV$ ) spectra. A wide-range voltage measurement was also performed in order to observe any QW-originated features in the conduction spectra. For the resonant sample, this measurement [Figs. 1(a) and 1(b)] revealed peaks with typical spacing. The peaks remained stationary with respect to temperature.

It can be seen that the spacing predicted by our model (presented below) is slightly larger than the experimental one. We attribute this difference to our model as it assumes linear rather than parabolic walls for the QW, thus resulting in a different spacing between the levels. Resonant features were absent in the conductance spectra of the nonresonant sample [Figs. 1(a) and 2(b)].

For the resonant sample, a zero-bias peak was observed, decreasing in magnitude as the temperature increases, disappearing at  $T_c$ . This zero-bias peak below  $T_c$  can be attributed to Andreev reflection. To study this effect in more detail, a higher resolution measurement [Fig. 2(a)] was then performed around the central peak which revealed more intricate features, including a triangular-shaped peak along with multiple dips, all having temperature dependence, disappearing above  $T_c$ . For the nonresonant sample, the conductance spectra exhibited a typical superconducting gap structure with two coherence peaks marking the edges of the gap [Fig. 2(b)]. Both features decreased in magnitude as the temperature increases, vanishing at  $T_c$ .

The theoretical model for the experimental observations is an extension of the Blonder-Tinkham-Klapwijk (BTK) model [28], taking into account the spatial nature of the

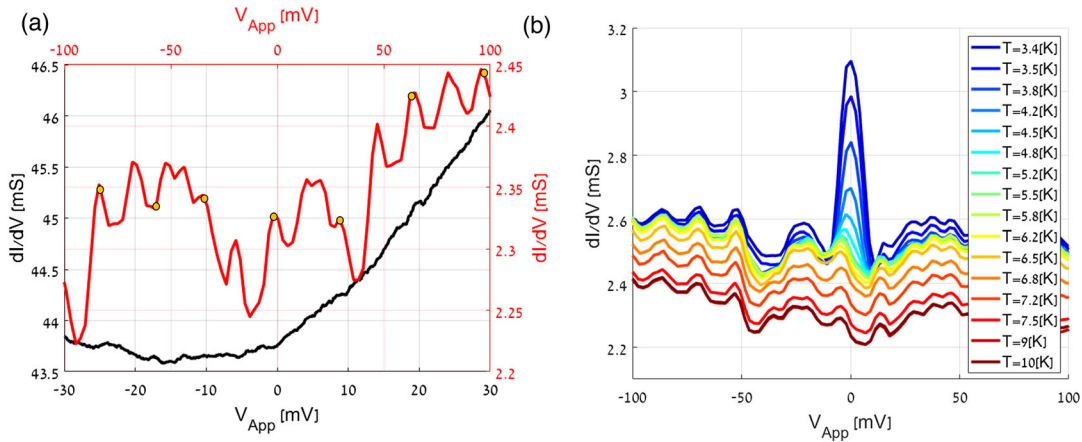


FIG. 1. (a) Measured conductance curves of the resonant device with a QW (red) and nonresonant device (black)—both above  $T_c$ . The resonant device curve exhibits a typically spaced structure resulting from the resonant levels in the QW, while the non resonant sample spectrum lacks such features. The resonant peaks are marked with yellow circles based on the theoretical model presented below. (b) Resonant sample conductance spectra for wide voltage ranges and temperatures. The two main features are repeating peaks and the central zero-bias peak. The periodic peaks do not change with temperature and are attributed to the resonant levels of the QW. The zero-bias peak is attributed to enhanced conductance caused by Andreev reflection.

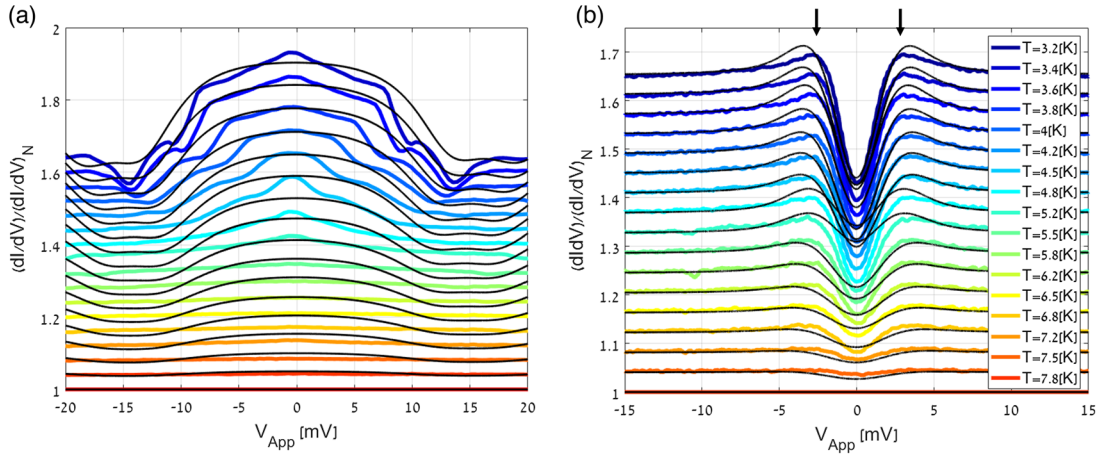


FIG. 2. (a),(b) Normalized device conductance spectra for the resonant (a) and nonresonant (b) samples with their respective calculated spectra. The curves are shifted vertically for clarity and the spectral features are broader than the superconducting gap due to series resistance of the PN junction. For the resonant sample, a central temperature-dependent peak can be observed. For the nonresonant sample, a superconducting gap, flanked by coherence peaks on both sides (black arrows) is observed. The nonresonant feature is readily explained by the BTK model (evident by the theoretical curves).

superconductor-semiconductor junction barrier [21]. A complete list of all fitting parameters used in our model appears in the Supplemental Material [29]. The BTK model describes the overall scattering of two quasiparticle wave functions satisfying the Bogoliubov–de Gennes equations:

$$\begin{aligned} \left[ -\frac{\hbar^2}{2m} - \mu(x) + V(x) \right] u(x) + \Delta(x)v(x) &= Eu(x), \\ -\left[ -\frac{\hbar^2}{2m} - \mu(x) + V(x) \right] v(x) + \Delta(x)u(x) &= Ev(x), \end{aligned} \quad (1)$$

With  $\mu(x)$ ,  $V(x)$ , and  $\Delta(x)$  being the chemical potential, potential barrier, and the superconducting order parameter, respectively, and  $u(x)$ ,  $v(x)$  being the quasiparticle wave functions. The BTK model makes the simplifying assumptions that  $\Delta(x) = \Delta_0\theta(x)$  where  $\theta(x)$  is the Heaviside function and the superconductor-semiconductor spatial potential is approximated to  $V(x) = H\delta(x)$  where  $H$  is the height of the barrier and  $\delta(x)$  is the Dirac delta function. Another useful parameter is the dimensionless barrier strength  $Z = H/\hbar v_f$ , where  $v_f$  is the Fermi velocity. For  $Z \rightarrow 0$  the barrier strength is reduced and Andreev reflection is dominant, while for a large  $Z$  Andreev reflection is inhibited in favor of quasiparticle tunneling.

Based on our previous work [21], the potential barrier  $V(x)$  and the superconducting order parameter  $\Delta(x)$  are split into segments, with each segment assigned a scattering matrix. The global scattering matrix is then obtained by multiplying the matrices governing each segment. The global matrix encodes any spatial dependence, which arises from either the barrier or the superconducting order parameter. Accounting for the scattering boundary conditions, the probabilities of reflecting a hole  $A(E)$  (Andreev reflection) or reflecting an electron  $B(E)$  (regular

reflection) can be calculated. As the device contains a one-sided QW, charge carriers that are injected into the QW and can only be reflected back or recombine. In order to avoid using non-Hermitian terms, in our model the PN junction has been replaced with a triangular potential of a given width and height [Fig. 3(b)], in order to simulate injection of charge carriers while still retaining a resonant structure. The overall  $I$ - $V$  and differential conductance ( $dI/dV$ ) spectra are obtained by the relations

$$\begin{aligned} I(V) &= C \int_{-\infty}^{\infty} [f_{\text{FD}}(E - eV) - f_{\text{FD}}(E)] \\ &\quad \times [1 + A(E) - B(E)] dE, \\ G(V) &= \frac{dI(V)}{dV} = C \int_{-\infty}^{\infty} \frac{d}{dV} [f_{\text{FD}}(E - eV)] \\ &\quad \times [1 + A(E) - B(E)] dE. \end{aligned} \quad (2)$$

Where  $C$  is a constant accounting for the junction area, Fermi velocity, density of states and charge, and  $f_{\text{FD}}$  is Fermi-Dirac distribution function.

In addition, special care was taken regarding the nonlinear resistive nature of our devices. Our devices contain both constant and nonlinear series resistance, the former originating from the thick  $p$ -type GaAs substrate and the latter originating from the PN junction adjacent to the superconductor-semiconductor contact. The effect of the constant series resistance is a uniform rescaling of both  $I$ - $V$  and differential conductance spectra due to voltage division between the substrate and the superconductor-semiconductor junction. The effect of the nonlinear PN junction resistance is more involved, resulting in nonuniform rescaling. Both the constant substrate resistance and the PN junction resistance were included in our theoretical

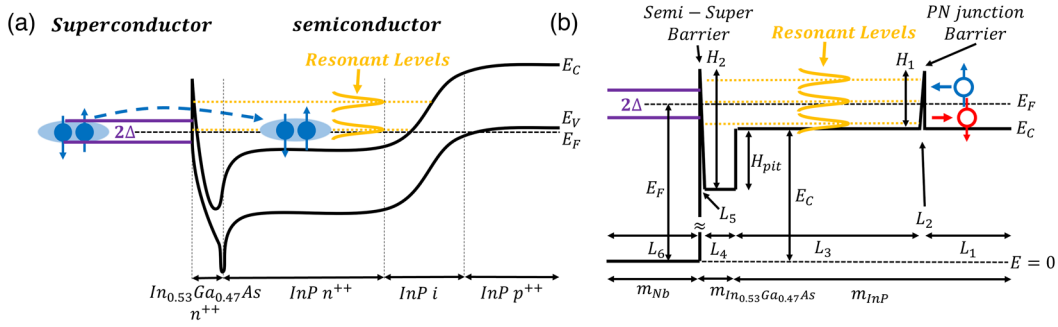


FIG. 3. (a) Schematic depiction of the device. Cooper pairs are injected from the superconductor into the PN junction. The confining nature of the  $n$ -type quantum well gives rise to resonant states. The semiconducting stack was designed so that the Fermi energy level overlaps with one of the resonant states, resulting in enhanced Cooper-pair injection. (b) Reduced diagram of the potential barrier used for the theoretical modeling. The PN junction has been replaced with a triangular potential barrier in order to retain the resonant structure while allowing for a standard Hermitian treatment of the problem.

model. In our experiments, the opaqueness of the junction was measured by superconducting-normal junction resistance, and the resistance of the resonant-level junction was in fact *higher* than that of the nonresonant junction ( $400\ \Omega$  vs  $12\ \Omega$ ) for the measured voltage range (several devices tested to ensure consistency). Moreover, the resonant features alone were found to have a peak-to-peak magnitude of  $50\ \Omega$ . Therefore, the interface alone in our samples was more opaque in the resonant structure, and the enhanced Andreev feature can be only explained by the resonant enhancement.

Since our model is based on the assumption that the particles modeled as wave functions without loss of coherence, understanding of the typical mean free path in our samples is crucial for the number of layers to be included in the modeling. As our sample is heavily doped to the point of being degenerate, carrier-carrier scattering in the quantum well is the dominant scattering mechanism. An earlier work by Snoke [34] detailed the dependence of the carrier scattering and thermalization rates on the dopant densities for GaAs. For dopant concentration of the order  $10^{19}\ \text{cm}^{-3}$ , a scattering time of  $\sim 100$  fs is obtained. Treating the  $\text{In}_{0.53}\text{Ga}_{0.47}\text{As}$  layer as a 3D degenerate semiconductor, the Fermi velocity is  $\sim 1.8 \times 10^6$  (m/s). The corresponding mean free path  $L_s$  is  $\sim 180$  nm. This scattering length implies that for the resonant sample, whose quantum well width is  $\sim 100$  nm, all layers that compose the quantum well should be taken into account in our model. For the nonresonant sample, as the thickness of the top  $\text{In}_{0.53}\text{Ga}_{0.47}\text{As}$  layer is  $\sim 300$  nm, it was the only layer taken into account in our model. The obtained mean free path of  $\sim 180$  nm also agrees with experimental results as for the resonant sample with  $\sim 100$  nm-wide quantum well, resonant features were observed while for the nonresonant sample with  $\sim 400$  nm-wide quantum well, resonant features were absent, indicating the typical mean free path for our samples should lie in the range of 100–400 nm.

For the resonant sample, using available device parameters (thickness, doping, layer composition, etc.), our theoretical

model has shown the presence of resonant levels with an original spacing of  $\sim 2\text{--}4$  meV (for a 100 nm QW) [29]. The larger broadening of  $\sim 20\text{--}25$  meV in the experimental data (Fig. 1), in comparison to the  $\sim 2\text{--}4$  meV broadening in our theoretical calculation, may arise from the quantum well being situated in series to a nonlinear PN junction, causing nonlinear rescaling of the conductance spectra feature width. The position of the Fermi energy level was shown [29] to approximately align with one of the resonant levels, resulting in enhanced Andreev features. The maximum enhancement of differential conductance (normalized to its value above  $T_c$ ) is 1.3. This enhancement of Andreev reflection in the junction can be explained by the presence of the resonant energy level, in good agreement with our model. The model, however, does not account for possible induced superconducting gap in the semiconductor in a proximity effect, which we believe is responsible for the double-gap Andreev spectra, as well as the triangular shape of the zero-bias peak [35]. Previous works [18,19] have demonstrated similar features, attributing them to the superconducting proximity effect inside the semiconducting layer.

For the nonresonant sample, no Andreev features in the differential conductance spectra were observed. Instead, a superconducting gap, accompanied by coherence peaks was obtained. This observation indicates that Andreev reflection is suppressed in favor of quasiparticle tunneling, indicated by reduction in conductance and accompanying coherence peaks. For both samples, the extracted value for the superconducting order parameter  $\Delta$  at 3 K was  $\sim 1$  meV which is close to the typical values reported for Nb [36] for both samples. The width of the zero-bias peak was also scaled due to the presence of the nonlinear PN junction and the resulting nonlinear voltage scaling, resulting in a much broader peak.

In conclusion, we have demonstrated enhancement of Andreev reflection through the use of resonant tunneling. This indicates an enhanced injection of Cooper pairs in our sample despite the presence of a relatively strong Schottky barrier. We have employed a numerical model extending the existing BTK model to include arbitrary spatial

potential barriers. Good agreement between theory and experiment was obtained for both our resonant and non-resonant samples. Our demonstration of semiconductor Cooper-pair injection enhancement by resonant tunneling paves the way for future superconductor-semiconductor-based quantum technologies and fundamental studies, including quantum optoelectronics, unique quantum Hall systems, and realizations of Majorana fermions.

The authors acknowledge funding from the Israel Science Foundation (ISF) through Grant No. 3581/21. We would like to acknowledge the Technion micro-nano fabrication unit (MNFU) for assisting us with the growth and fabrication of our devices, especially Dr. Guy Ankonina from the Photovoltaics lab working under the Russell Berrie nanotechnology institute (RBNI) and the Grand Technion Energy Program (GTEP).

- 
- [1] M. Tinkham, *Introduction to Superconductivity*, 2nd ed. (McGraw-Hill, New York, 1996).
- [2] I. Suemune, T. Akazaki, K. Tanaka, M. Jo, K. Uesugi, M. Endo, H. Kumano, E. Hanamura, H. Takayanagi, M. Yamanishi, and H. Kan, Superconductor-based quantum-dot light-emitting diodes: Role of Cooper pairs in generating entangled photon pairs, *Jpn. J. Appl. Phys.* **45**, 9264 (2006).
- [3] M. Khoshnegar and A. H. Majedi, Entangled photon pair generation in hybrid superconductor-semiconductor quantum dot devices, *Phys. Rev. B* **84**, 104504 (2011).
- [4] E. Sabag, S. Bouscher, R. Marjeh, and A. Hayat, Photonic bell-state analysis based on semiconductor-superconductor structures, *Phys. Rev. B* **95**, 094503 (2017).
- [5] R. Marjeh, E. Sabag, and A. Hayat, Light amplification in semiconductor-superconductor structures, *New J. Phys.* **18**, 023019 (2016).
- [6] Z. Wan, A. Kazakov, M. J. Manfra, L. N. Pfeiffer, K. W. West, and L. P. Rokhinson, Induced superconductivity in high-mobility two-dimensional electron gas in gallium arsenide heterostructures, *Nat. Commun.* **6**, 7426 (2015).
- [7] C. Reeg, D. Loss, and J. Klinovaja, Proximity effect in a two-dimensional electron gas coupled to a thin superconducting layer, *Beilstein J. Nanotechnol.* **9**, 1263 (2018).
- [8] K. Delfanazari, R. K. Puddy, P. Ma, T. Yi, M. Cao, Y. Gul, I. Farrer, D. A. Ritchie, H. J. Joyce, M. J. Kelly, and C. G. Smith, Proximity induced superconductivity in indium gallium arsenide quantum wells, *J. Magn. Magn. Mater.* **459**, 282 (2018).
- [9] M. Kjaergaard, F. Nichele, H. J. Suominen, M. P. Nowak, M. Wimmer, A. R. Akhmerov, J. A. Folk, K. Flensberg, J. Shabani, C. J. Palmstrøm, and C. M. Marcus, Quantized conductance doubling and hard gap in a two-dimensional semiconductor-superconductor heterostructure, *Nat. Commun.* **7**, 12841 (2016).
- [10] M. Hell, K. Flensberg, and M. Leijnse, Coupling and braiding Majorana bound states in networks defined in two-dimensional electron gases with proximity-induced superconductivity, *Phys. Rev. B* **96**, 035444 (2017).
- [11] F. Deon, V. Pellegrini, F. Giazotto, G. Biasiol, L. Sorba, and F. Beltram, Proximity effect in a two-dimensional electron gas probed with a lateral quantum dot, *Phys. Rev. B* **84**, 100506(R) (2011).
- [12] S. S. Mou, H. Irie, Y. Asano, K. Akahane, H. Kurosawa, H. Nakajima, H. Kumano, M. Sasaki, and I. Suemune, Superconducting light-emitting diodes, *IEEE J. Sel. Top. Quantum Electron.* **21**, 7900111 (2015).
- [13] S. S. Mou, H. Irie, Y. Asano, K. Akahane, H. Nakajima, H. Kumano, M. Sasaki, A. Murayama, and I. Suemune, Optical observation of superconducting density of states in luminescence spectra of InAs quantum dots, *Phys. Rev. B* **92**, 035308 (2015).
- [14] I. Suemune, Y. Hayashi, S. Kuramitsu, K. Tanaka, T. Akazaki, H. Sasakura, R. Inoue, H. Takayanagi, Y. Asano, E. Hanamura, S. Odashima, and H. Kumano, A Cooper-pair light-emitting diode: Temperature dependence of both quantum efficiency and radiative recombination lifetime, *Appl. Phys. Express* **3**, 054001 (2010).
- [15] A. Hayat, H. Y. Kee, K. S. Burch, and A. M. Steinberg, Cooper-pair-based photon entanglement without isolated emitters, *Phys. Rev. B* **89**, 094508 (2014).
- [16] A. Kastalsky, A. W. Kleinsasser, L. H. Greene, R. Bhat, F. P. Milliken, and J. P. Harbison, Observation of Pair Currents in Superconductor-Semiconductor Contacts, *Phys. Rev. Lett.* **67**, 3026 (1991).
- [17] C. Nguyen, H. Kroemer, and E. L. Hu, Anomalous Andreev Conductance in InAs-AlSb Quantum Well Structures with Nb Electrodes, *Phys. Rev. Lett.* **69**, 2847 (1992).
- [18] T. Nishino, M. Hatano, H. Hasegawa, T. Kure, and F. Murai, Carrier reflection at the superconductor-semiconductor boundary observed using a coplanar-point-contact injector, *Phys. Rev. B* **41**, 7274 (1990).
- [19] D. R. Heslinga, S. E. Shafranjuk, H. van Kempen, and T. M. Klapwijk, Observation of double-gap-edge Andreev reflection at Si/Nb interfaces by point-contact spectroscopy, *Phys. Rev. B* **49**, 10484 (1994).
- [20] D. Panna, S. Bouscher, K. Balasubramanian, V. Perepelock, S. Cohen, D. Ritter, and A. Hayat, Andreev reflection in a superconducting light-emitting diode, *Nano Lett.* **18**, 6764 (2018).
- [21] S. Bouscher, R. Winik, and A. Hayat, Andreev reflection enhancement in semiconductor-superconductor structures, *Phys. Rev. B* **97**, 054512 (2018).
- [22] P. Rickhaus, M. Weiss, L. Marot, and C. Schönenberger, Quantum Hall effect in graphene with superconducting electrodes, *Nano Lett.* **12**, 1942 (2012).
- [23] D. J. Clarke, J. Alicea, and K. Shtengel, Exotic non-Abelian anyons from conventional fractional quantum Hall states, *Nat. Commun.* **4**, 1348 (2013).
- [24] L. L. Chang, L. Esaki, and R. Tsu, Resonant tunneling in semiconductor double barriers, *Appl. Phys. Lett.* **24**, 593 (1974).
- [25] J. P. Sun, G. I. Haddad, P. Mazumder, and J. N. Schulman, Resonant tunneling diodes: Models and properties, *Proc. IEEE* **86**, 641 (1998).
- [26] J. Faist, F. Capasso, D. L. Sivco, C. Sirtori, A. L. Hutchinson, and A. Y. Cho, Quantum cascade laser, *Science* **264**, 553 (1994).
- [27] K. Kajiyama, Y. Mizushima, and S. Sakata, Schottky barrier height of  $n$ -In<sub>x</sub>Ga<sub>1-x</sub>As diodes, *Appl. Phys. Lett.* **23**, 458 (1973).

- [28] G. E. Blonder, M. Tinkham, and T. M. Klapwijk, Transition from metallic to tunneling regimes in superconducting microconstrictions: Excess current, charge imbalance, and supercurrent conversion, *Phys. Rev. B* **25**, 4515 (1982).
- [29] See Supplemental Material at <http://link.aps.org/supplemental/10.1103/PhysRevLett.128.127701> which also includes Refs. [30–33], for extended description of the theoretical model and fitting parameters.
- [30] L. F. Mattheiss, Electronic structure of niobium and tantalum, *Phys. Rev. B* **1**, 373 (1970).
- [31] D. Schneider, D. Rürup, A. Plichta, H.-U. Grubert, A. Schlachetzki, and K. Hansen, Shubnikov–de Haas effect and effective mass in  $n$ -InP in dependence on carrier concentration, *Z. Phys. B* **95**, 281 (1994).
- [32] D. Schneider, L. Elbrecht, J. Creutzburg, A. Schlachetzki, and G. Zwinge, In-plane effective mass of electrons in InGaAs/InP quantum wells, *J. Appl. Phys.* **77**, 2828 (1995).
- [33] D. P. Karim, J. B. Ketterson, and G. W. Crabtree, A de Haas–van Alphen study of niobium: Fermi surface, cyclotron effective masses, and magnetic breakdown effects, *J. Low Temp. Phys.* **30**, 389 (1978).
- [34] D. W. Snoke, Density dependence of electron scattering at low density, *Phys. Rev. B* **50**, 11583 (1994).
- [35] G. J. Strijkers, Y. Ji, F. Y. Yang, C. L. Chien, and J. M. Byers, Andreev reflections at metal/superconductor point contacts: Measurement and analysis, *Phys. Rev. B* **63**, 104510 (2001).
- [36] A. V. Pronin, M. Dressel, A. Pimenov, A. Loidl, I. V. Roshchin, and L. H. Greene, Direct observation of the superconducting energy gap developing in the conductivity spectra of niobium, *Phys. Rev. B* **57**, 14416 (1998).